Theory of metal-insulator transition in the family of perovskite iridium oxides

Jean-Michel Carter,[1] Vijay Shankar V.,[1] and Hae-Young Kee[1,2,*]
[1]*Department of Physics, University of Toronto, Toronto, Ontario, Canada M5S 1A7*
[2]*Canadian Institute for Advanced Research, Toronto, Ontario, Canada*
(Received 18 April 2013; published 9 July 2013)

Perovskite iridium oxides $Sr_{n+1}Ir_nO_{3n+1}$ exhibit fascinating phenomena due to the combined effects of spin-orbit coupling (SOC) and electronic interactions. It was suggested that electronic correlation amplified via the strong SOC leads to a spin-orbit Mott insulator for $n = 1$ and 2, while three-dimensional (3D) $SrIrO_3$ remains metallic because of the large bandwidth from the 3D structure. However, this bandwidth-controlled metal-insulator transition (MIT) is only valid when SOC is large enough to split $J_{\text{eff}} = 1/2$ and $3/2$ bands, while the mixing of $1/2$ and $3/2$ bands is conspicuous among the occupied bands. Here, we investigate the MIT as a function of n using weak-coupling theory. In this approach, the magnetic instability is determined by the states near the Fermi level rather than the entire band structure. Starting from t_{2g} tight-binding models for $n = 1, 2$, and ∞, the states near the Fermi level are found to be predominantly $J_{\text{eff}} = 1/2$ allowing an effective single-band model. Supplementing this effective $J_{\text{eff}} = 1/2$ model with Hubbard-type interactions, transitions from a metal to magnetically ordered states are obtained. Strong-coupling spin models are derived to compare the magnetic ordering patterns obtained in the weak- and strong-coupling limits. We find that they are identical, indicating that these iridates are likely in an intermediate-coupling regime.

DOI: 10.1103/PhysRevB.88.035111 PACS number(s): 71.30.+h, 71.70.Ej, 75.30.Kz

I. INTRODUCTION

Spin-orbit coupling (SOC) is often either ignored or treated perturbatively in correlated electronic materials where $3d$ or $4d$ orbitals are active. However, in materials with heavier atoms, SOC plays an important role in determining the ground state and often helps stabilize novel phases such as topological insulators[1,2] and spin liquids.[3] In particular, the interplay between SOC and electronic interactions needs to be understood when these energy scales are comparable. Iridium oxides (iridates) with $5d$ orbitals offer a playground to investigate their combined effects.[4–11]

In the Ruddlesden-Popper series of iridium oxides, $Sr_{n+1}Ir_nO_{3n+1}$, an octahedral crystal field due to oxygen atoms separates the e_g and t_{2g} states, leaving five electrons on the t_{2g} levels. When SOC is large, these t_{2g} states are split into $J_{\text{eff}} = 1/2$ and $3/2$, and the system can be viewed as half-filled, $J_{\text{eff}} = 1/2$. Since the bandwidth of $J_{\text{eff}} = 1/2$, W_j, is narrower than the original bandwidth $W_{t_{2g}}$ of all the t_{2g} states without SOC, the Hubbard interaction U on the half-filled $J_{\text{eff}} = 1/2$ state is effectively enhanced, as the ratio U/W_j is larger than $U/W_{t_{2g}}$. Thus the effect of Hubbard interaction in iridates is amplified due to strong SOC via a narrowing of the bandwidth, leading to an insulating state in some layered perovskite[12–19] and pyrochlore[6,7] iridates. This state, dubbed a spin-orbit Mott insulator, was first reported in single-layered perovskite Sr_2IrO_4 (Sr-214).[16,17,19]

This idea of narrowing the bandwidth was applied to explain the insulator-metal transition in $Sr_{n+1}Ir_nO_{3n+1}$ series as a function of n. While single-layer Sr_2IrO_4 (Sr-214) with $n = 1$ and bilayer $Sr_3Ir_2O_7$ (Sr-327) with $n = 2$ are insulators, three-dimensional $SrIrO_3$ (Sr-113) with $n = \infty$ is metallic.[17] Since the $J_{\text{eff}} = 1/2$ state made of an equal mixture of d_{xy}, d_{xz}, and d_{yz} orbitals is almost isotropic, Sr-113 has a larger bandwidth than the layered compounds Sr-214 and Sr-327. U/W_j is smaller in Sr-113, which then leads to a metallic state in Sr-113. Sr-327, via analogous reasoning, is closer to a transition from a metal to an insulator with a smaller charge gap than Sr-214. This mechanism was referred to as a dimensionality-controlled metal-insulator transition (MIT).[17]

The above proposal, however, is only valid when SOC is large enough to split $J_{\text{eff}} = 1/2$ and $3/2$ bands. Once these two bands are well separated, W_j increases as n increases, and one can compare it with the Hubbard interaction U. In the opposite limit, without SOC, the original t_{2g} bandwidth $W_{t_{2g}}$ is not very sensitive to the dimensionality. Therefore, the dimensionality-controlled MIT scenario strongly depends on the strength of SOC. With this in mind, it is important to notice recent experimental and theoretical developments. Multiple angle-resolved photoemission spectroscopy (ARPES) measurements,[16,20,21] *ab initio* calculations,[22,23] and a tight-binding theory of Sr-214 and Sr-327 (Ref. 24) report that these two bands are not well separated, and the mixing between $J_{\text{eff}} = 1/2$ and $3/2$ is not negligible among the occupied bands.

When SOC is intermediate, close to the values deduced from *ab initio* calculations and ARPES, W_j is not well-defined, and the occupied bands are a mixture of $J_{\text{eff}} = 1/2$ and $3/2$. As the dimensionality n is increased, the mixing between $1/2$ and $3/2$ among the occupied bands increases. The actual bandwidth W in the case of intermediate SOC is larger than $W_{t_{2g}}$ due to the effect of spin-orbit coupling. The estimated Hubbard U is smaller than this bandwidth W, and a strong-coupling Mott insulator scheme is questionable. It was pointed out by Arita *et al.*[23] that Sr-214 is a Slater rather than a Mott insulator. Given that the magnetic structure does not break any further translational symmetry, unlike a typical Slater insulator, the Slater behavior is not immediately apparent. Thus an understanding of the MIT and how it is associated with the magnetic ordering in the family of iridates within the Slater scheme is a pertinent question.

In this paper, we study the MIT as a function of the number of layers in a unit cell within the Slater picture. If the Slater picture is appropriate, this approach should reveal a MIT in

the layered iridates. To proceed, the states near the Fermi level rather than all the occupied states need to be identified, since the magnetic instability is determined by states near the Fermi level within the weak-coupling approach. While the mixing between $J_{\rm eff} = 1/2$ and $3/2$ is large for the occupied states, the states near the Fermi level are mainly $J_{\rm eff} = 1/2$ for the case of intermediate SOC. Thus, we carry out a mean-field study of a Hubbard model for the $J_{\rm eff} = 1/2$ bands near E_F. The density of states (DOS) near the Fermi level is inherited from the point-group symmetry of the crystal structure, and not simply determined by the dimensionality of crystal structure. Our results imply that the combination of SOC and the crystal structure plays an important role in determining the different magnetic ordering patterns for this series of iridates. In turn, we suggest that the pattern of magnetic ordering and the size of the magnetic moment in the insulating phase can be sensitive to changes in crystal structure. While the magnetic ordering itself is a consequence of electronic correlations and should not be sensitive to the details, this does not guarantee a Mott insulator, as will be discussed below.

The paper is organized as follows. In Sec. II, we introduce a tight-binding model with SOC using t_{2g} orbitals for the different layered iridates. From this model, we identify the states near the Fermi level as being comprised of mostly $J_{\rm eff} = 1/2$ orbitals. Then, in Sec. III we discuss an effective tight-binding model using $J_{\rm eff} = 1/2$ orbitals that reproduces the band structure near the Fermi level. We then study the effect of interactions at a mean-field level using an effective Hubbard model for these orbitals. The magnetic states obtained using a self-consistent method are then explained in Sec. IV. A collinear antiferromagnetic (AF) state with moments oriented along the crystal c axis is found in Sr-327, while a coplanar canted AF is realized in Sr-214. The full unit-cell structure in Sr-214 breaks spin-rotation symmetry and favors the canted AF state, while the bilayer structure determines the collinear AF state in Sr-327. Sr-113, although close to a magnetic transition, remains metallic because interactions in the real material are smaller than the critical interaction strength required for this magnetic transition. The results found at the mean-field level are compared with spin models derived in the strong-coupling limit in Sec. V. Finally, we discuss the implications of our results and conclude in Sec. VI.

II. TIGHT-BINDING MODEL WITH t_{2g} ORBITALS

In the layered Ruddelsden-Popper series of iridates, the oxidation state of iridium is Ir^{4+} with an electronic configuration of $[Xe]5d^5$. The octahedral crystal field from the oxygen atoms further splits the $5d$ levels into triply degenerate t_{2g} and doubly degenerate e_g levels with t_{2g} lying lower in energy. There are then five d electrons in the t_{2g} levels. Iridium, being a heavy atom, has significant spin-orbit coupling. Within the low-lying t_{2g} subspace, the orbital angular momentum behaves like an effective angular momentum $l = 1$ with a negative spin-orbit coupling constant λ.[25] With this picture of the atomic levels in iridium, tight-binding models incorporating SOC within the t_{2g} orbitals d_{yz}, d_{xz}, and d_{xy} are discussed for the different layered iridates.

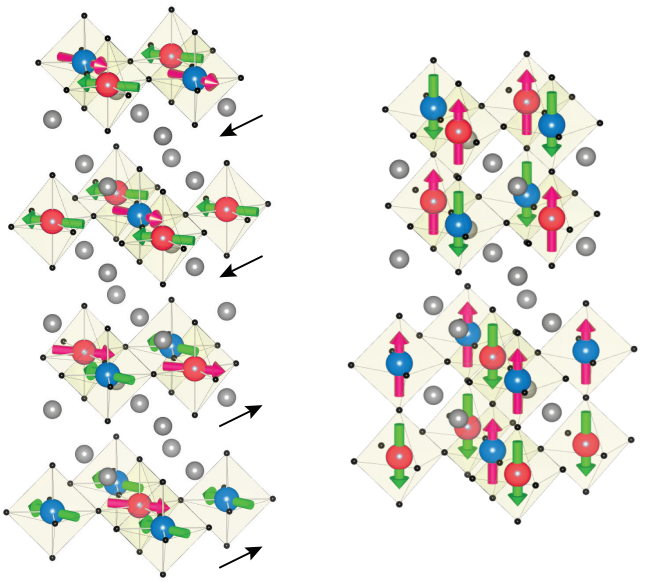

(a) (b)

FIG. 1. (Color online) Theoretical magnetic ordering in Sr-214 (a) and Sr-327 (b) in the insulating phase. Each layer has two different iridium atoms because of the staggered rotation of the octahedra, which we label blue and red. (a) The coplanar canted AF state is shown with the spin configuration for each layer. The black arrow represents the direction of the net ferromagnetic moment within each plane, showing the up-up-down-down structure. (b) The favored collinear AF state with moments pointing along the c axis is shown; the second bilayer has its spins flipped from the first set.

A. Tight-binding model for Sr-214

Sr-214 is a layered compound with a unit cell that contains four layers. Within each layer, the oxygen octahedra rotate about the c axis in a staggered fashion contributing two Ir atoms [which we label blue (B) and red (R)] to the unit cell, as shown in Fig. 1(a). For the sake of clarity, although the actual unit cell has eight Ir atoms, we focus on a single IrO_2 layer with two Ir atoms in this section. The hoppings between the various layers will be discussed later in Sec. III.

Let $d^{\dagger,\gamma,\alpha}_{k,\sigma}$ denote the creation operator for an electron with spin $\sigma = \uparrow,\downarrow$ and orbital $\alpha = yz,xz,xy$ in sublattice $\gamma =$ blue (B), red (R). Using the spinor $\psi_k = [d^{B,yz}_{k,\downarrow}, d^{B,xz}_{k,\downarrow}, d^{B,xy}_{k,\uparrow}, B \leftrightarrow R, \uparrow\leftrightarrow\downarrow]^T$, we can write the tight-binding Hamiltonian as $\sum_k \psi^\dagger_k H \psi_k$. Considering both nearest-neighbor (NN) and next-nearest-neighbor (NNN) hoppings, the matrix H in this basis is given by

$$H = \begin{pmatrix} H_{\rm so} + H_{BB} & H_{BR} \\ H^\dagger_{BR} & H_{\rm so} + H_{RR} \end{pmatrix} + [\uparrow\leftrightarrow\downarrow], \qquad (1)$$

where $H_{\rm so}$, the atomic spin-orbit coupling $\lambda \boldsymbol{L}_i \cdot \boldsymbol{S}_i$, is

$$H_{\rm so} = \begin{pmatrix} 0 & i\lambda/2 & -\lambda/2 \\ -i\lambda/2 & 0 & i\lambda/2 \\ -\lambda/2 & -i\lambda/2 & 0 \end{pmatrix}. \qquad (2)$$

H_{BR} and $H_{BB/RR}$ represent the NN and NNN hopping matrices, respectively, and are given by

$$H_{BR} = \begin{pmatrix} \epsilon_n^{yz} & \epsilon^{\rm rot} & 0 \\ -\epsilon^{\rm rot} & \epsilon_n^{xz} & 0 \\ 0 & 0 & \epsilon_n^{xy} \end{pmatrix}, \quad H_{BB/RR} = \begin{pmatrix} \epsilon_d^{yz} & \epsilon^{1d} & 0 \\ \epsilon^{1d} & \epsilon_d^{xz} & 0 \\ 0 & 0 & \epsilon_d^{xy} \end{pmatrix}, \tag{3}$$

where the dispersions ϵ_n^{yz}, ϵ_n^{xz}, $\epsilon^{\rm rot}$, ϵ_n^{xy}, ϵ_d^{yz}, ϵ_d^{xz}, ϵ^{1d}, and ϵ_d^{xy} are listed in Appendix A.

B. Tight-binding model for Sr-327

Sr-327, like Sr-214, has a layered structure with a unit cell that spans four layers. Unlike Sr-214, Sr-327 has a bilayer structure with two bilayers as shown in Fig. 1(b) in the unit cell.[27] Each layer resembles Sr-214 with its staggered oxygen octahedra rotation, and the stacking is such that octahedra neighboring each other in adjacent layers of a bilayer rotate in opposite directions. A single bilayer with four Ir atoms is considered for the t_{2g} tight-binding model. The middle panel in Fig. 2(e) was used to study the magnetic ordering mechanism for Sr-327.[24] Starting from a three-band t_{2g} model, it was found that the magnetic ordering occurs mainly in the $J_{\rm eff} = 1/2$ band near the Fermi level.

Following previously employed notation, a spinor $\psi_{k,l} = [d^{l,B,yz}_{k,\downarrow}, d^{l,B,xz}_{k,\downarrow}, d^{l,B,xy}_{k,\uparrow}, B \leftrightarrow R, \uparrow\leftrightarrow\downarrow]^T$, where the additional

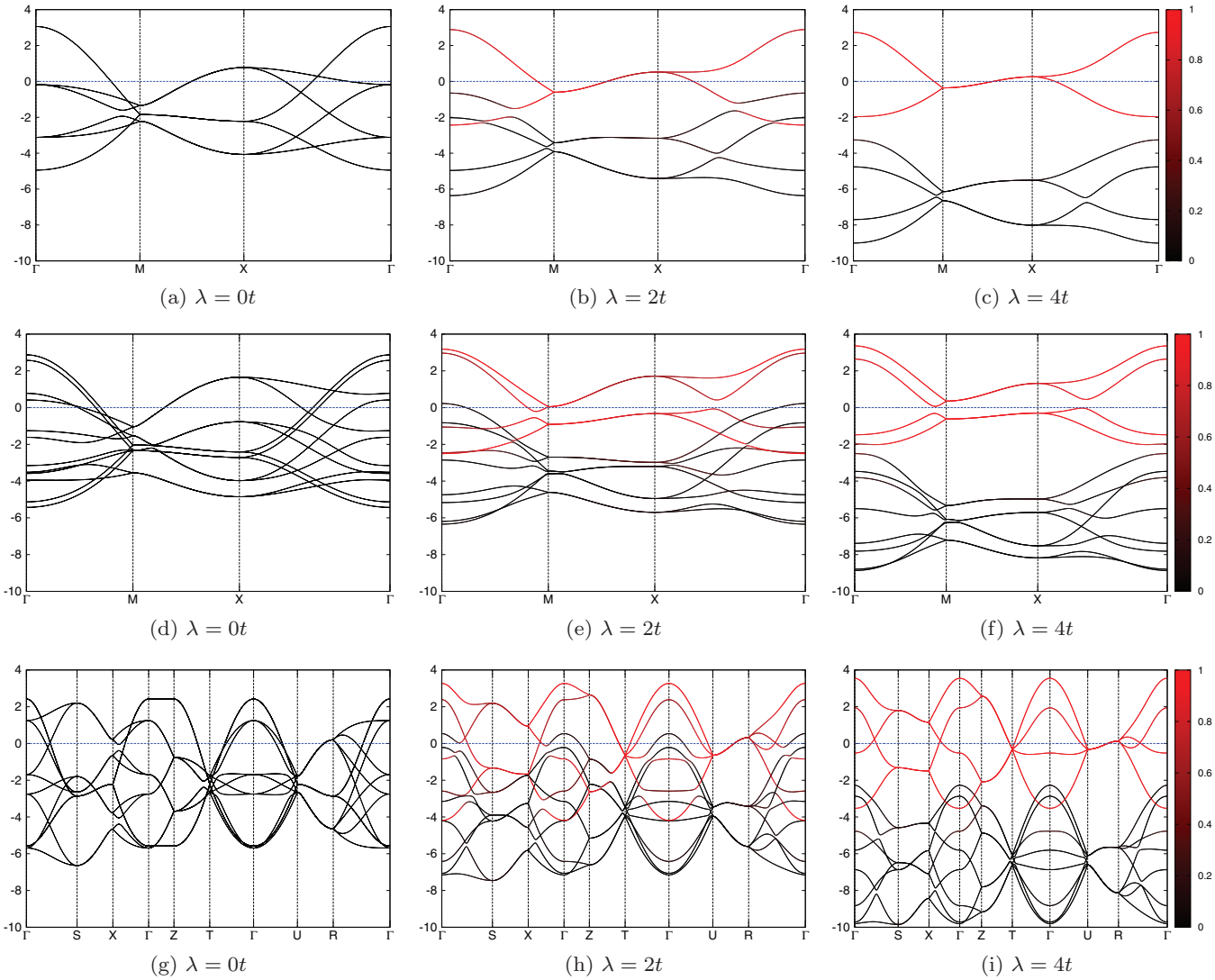

FIG. 2. (Color online) Tight-binding band structure using t_{2g} orbitals for Sr-214 (first row), Sr-327 (second row), and Sr-113 (third row) as a function of SOC strength λ. Red is used to indicate the weight of $J_{\rm eff} = 1/2$ orbitals in each band, and the blue horizontal line denotes the Fermi level. For intermediate λ (second column), the $J_{\rm eff} = 1/2$ bands are not separated from the $J_{\rm eff} = 3/2$ bands. In Sr-113, the tilting of the oxygen octahedra in addition to rotation leads to four Ir atoms in a unit cell.[26] Here, to enable comparison, the Brillouin zone is folded with a wave vector $Q = (0,0,\pi)$, but the effect of tilting of the oxygen octahedra on the band degeneracy is not included for simplicity.

index $l = 1,2$ denotes the two different layers in the bilayer, is employed to write the tight-binding Hamiltonian as $\sum_k \psi^\dagger_{k,l} H^{ll'} \psi_{k,l'}$. Including up to NNN hoppings, the matrix H is given by

$$H^{ll'} = \begin{pmatrix} H_{\rm so}\delta_{ll'} + H^{ll'}_{BB} & H^{ll'}_{BR} \\ H^{\dagger ll'}_{BR} & H_{\rm so}\delta_{ll'} + H^{ll'}_{BB} \end{pmatrix} + [\uparrow \leftrightarrow \downarrow], \quad (4)$$

with $l = l'$ reproducing the Hamiltonian for Sr-214 discussed in the previous section. $l \neq l'$ is the hopping between the layers and consists of two parts,

$$H^{12}_{BR} = \begin{pmatrix} t_z & t'_z & 0 \\ -t'_z & t_z & 0 \\ 0 & 0 & t^\delta_z \end{pmatrix}, \quad H^{12}_{BB} = \begin{pmatrix} \epsilon^{yz}_b & 0 & 0 \\ 0 & \epsilon^{xz}_b & 0 \\ 0 & 0 & 0 \end{pmatrix}, \quad (5)$$

where the first part H^{12}_{BR} includes hopping from a blue atom to a red atom immediately on top of it and the second part H^{12}_{BB} denotes hopping from a blue atom to the four nearest blue atoms on the adjacent layer. In the first part, t_z, t'_z, and t^δ_z represent the intraorbital hopping for $d_{yz\,(xz)}$ orbitals, hopping from a d_{yz} orbital to a d_{xz} orbital, and hopping between d_{xy} orbitals, respectively. The dispersions ϵ^{yz}_b,ϵ^{xz}_b, in H^{12}_{BB} are described in Appendix A 2.

C. Tight-binding model for Sr-113

Sr-113 is a three-dimensional compound which crystallizes in an orthorhombic perovskite structure under pressure.[28,29] The oxygen octahedra surrounding the Ir atoms are rotated about the z axis and tilted about the [110] direction in such a way that there are four different Ir atoms in the unit cell. Here, for the sake of simplicity,[41] we will not include the tilting of the octahedra along the [110] direction. In the same spinor basis used for Sr-214, the tight-binding Hamiltonian is

$$H = \begin{pmatrix} H_{\rm so} + H_{BB} + H_z & H_{BR} \\ H^\dagger_{BR} & H_{\rm so} + H_{RR} + H_z \end{pmatrix} + [\uparrow \leftrightarrow \downarrow], \quad (6)$$

with H_{BB} and H_{RR} identical to Sr-214 and the additional matrix H_z denoting c-axis dispersions given by

$$H_z = \begin{pmatrix} \epsilon_z & 0 & 0 \\ 0 & \epsilon_z & 0 \\ 0 & 0 & \epsilon^\delta_z \end{pmatrix}. \quad (7)$$

Here, ϵ_z and ϵ^δ_z denote intraorbital hopping along the c axis for $d_{yz/xz}$ and d_{xy} orbitals, respectively, as shown in Appendix A 3.

The band structures for Sr-214, Sr-327, and Sr-113 are plotted in Fig. 2. The three rows in the figure represent Sr-214, Sr-327, and Sr-113, respectively. The three columns represent no SOC, intermediate SOC, and large SOC, respectively. The $J_{\rm eff} = 1/2$ bands in columns 2 and 3 have been colored red. When SOC is absent (column 1), increasing the dimensionality does not have a significant effect on the bandwidth of the t_{2g} orbitals, as mentioned in the Introduction. For spin-orbit coupling large enough to separate the $J_{\rm eff} = 1/2$ orbitals from the $J_{\rm eff} = 3/2$ orbitals (column 3), the bandwidth does increase with dimensionality. With intermediate SOC (column 2), the occupied states are a mixture of $J_{\rm eff} = 1/2$ and $3/2$, and the $J_{\rm eff} = 1/2$ bandwidth W_j is not well-defined for this case. From the colors, we can infer that while there is significant mixing between $J_{\rm eff} = 1/2$ and $3/2$, the bands near the Fermi level are mostly comprised of $J_{\rm eff} = 1/2$ orbitals. Note that SOC in combination with the bilayer hopping makes Sr-327 almost insulating with a direct gap at every k point. This intermediate-coupling band structure is also consistent with those seen in LDA + SOC calculations. Within the weak-coupling approach, the magnetic instability is mainly determined by the states proximate to the Fermi level. Having identified these bands to be mostly composed of $J_{\rm eff} = 1/2$ orbitals, an effective tight-binding model for the three compounds is derived below.

III. TIGHT-BINDING MODEL IN THE $J_{\rm eff} = \frac{1}{2}$ BASIS

Within weak-coupling theory, bands near the Fermi level rather than all bands are relevant, and the states near the Fermi-level are made up of mostly $J_{\rm eff} = 1/2$ orbitals, as shown in the previous section. Thus an effective Hamiltonian for the $J_{\rm eff} = 1/2$ orbitals is obtained by changing to the angular momentum J basis and projecting out states not belonging to $J_{\rm eff} = 1/2$. The $J_{\rm eff} = 1/2$ states are given by

$$\left| J_z = \pm\frac{1}{2} \right\rangle = \frac{1}{\sqrt{3}}(|d_{yz}, \mp s\rangle \pm i|d_{xz}, \mp s\rangle \pm |d_{xy}, \pm s\rangle), \quad (8)$$

where $s = \pm$ denotes the spin of the electron.

In the $J_{\rm eff} = 1/2$ basis, a time-reversal invariant hopping Hamiltonian for a bond is of the form

$$t\sigma_0 + i \sum_{\alpha=x,y,z} t^\alpha \sigma^\alpha, \quad (9)$$

where the σ Pauli matrices represent the pseudospin degree of freedom. To a first approximation, the parameters t and t^α can be derived from the t_{2g} hoppings, as done in Appendix B.

As previously mentioned, the unit cell of Sr-214 is comprised of four distinct layers with two sublattices in each layer. Here, we include all the layers and use a spinor basis $\phi^l_k = (c^{lB}_{k+}, c^{lB}_{k-}, c^{lR}_{k+}, c^{lR}_{k-})^T$ to represent our Hamiltonian, where $l = 1,2,3,4$ denotes the layer, B,R are the two sublattices in each layer, and $+,-$ represent the pseudospin states $J_z = 1/2$ and $-1/2$, respectively.

Restricting ourselves to hoppings within a layer and between adjacent layers, the Hamiltonian can be written as $H_0 = \sum_k \phi^{\dagger l}_k H^{ll'}_k \phi^{l'}_k$, where

$$H^{ll'}_k = \begin{pmatrix} A_k & B_k & 0 & e^{ik_z c} C^\dagger_k \\ B^\dagger_k & A_k & C_k & 0 \\ 0 & C^\dagger_k & A_k & B_k \\ e^{-ik_z c} C_k & 0 & B^\dagger_k & A_k \end{pmatrix}. \quad (10)$$

Here c is the c-axis lattice constant, and A_k, B_k, and C_k are each 4×4 matrices with A_k having all the intralayer hoppings, B_k containing interlayer hoppings between layers 1 and 2 (3 and 4), and C_k containing hoppings between layers 2 and 3 (4 and 1). A single-layer model would only have A_k.

Using Pauli matrices τ to represent the sublattice degree of freedom and σ to represent the pseudospin, the different hopping matrices are given by

$$A_k = \epsilon^a_k + \epsilon^{ad}_k \tau_x + \epsilon'^{ad}_k \tau_y \sigma_z, \quad (11)$$

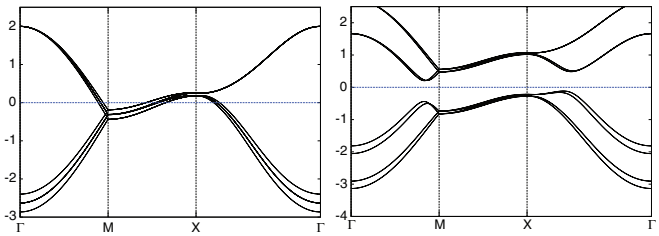

(a) Sr-214 (b) Sr-327

FIG. 3. (Color online) Band structure for the $J_{\rm eff} = 1/2$ tight-binding model for (a) Sr-214 and (b) Sr-327. At the Fermi level, this is consistent with the LDA calculation and the t_{2g} tight-binding model, shown in the third column of Fig. 2. In contrast to Fig. 2, the full unit cell including the four layers for Sr-214 and the two bilayers for Sr-327 is considered here.

$$B_k = \epsilon_k^b + \epsilon_k^{bd}\tau_x + \epsilon_k^{bz}\tau_y\sigma_z + \epsilon_k^{by}\tau_y\sigma_y + \epsilon_k^{bx}\tau_y\sigma_x, \quad (12)$$

$$C_k = \epsilon_k^c + \epsilon_k^{cd}\tau_x + \epsilon_k^{cz}\tau_y\sigma_z + \epsilon_k^{cy}\tau_y\sigma_y + \epsilon_k^{cx}\tau_y\sigma_x, \quad (13)$$

where the various dispersions making up A_k, B_k, and C_k are given in Appendix B 1a.

The noninteracting Hamiltonian in the $J_{\rm eff} = 1/2$ for Sr-327 is similar to that for Sr-214 in Eq. (10), with identical matrices A_k and C_k. The bilayer nature of this material makes B_k very different. Instead of weak interlayer hopping terms, there are large bilayer hoppings of the form $B_k = t_c\tau_x + t_c'\tau_y\sigma_x$, where t_c represents the hopping from a blue (red) atom to a red (blue) atom with the same J_z, and t_c' is the hopping from an orbital on a blue (red) atom to an orbital on a red (blue) atom with different J_z. The underlying band structure for this compound is shown in Fig. 3(b) and the parameters used are given in Appendix B 1b. The important difference between Sr-327 and Sr-214 is that, for any set of parameters, Sr-327 has a direct gap at each wave vector. The difference in the nature of the magnetic transition for the Hubbard model can be traced back to this feature of the band structure.

The $J_{\rm eff} = 1/2$ model for the three-dimensional compound Sr-113 has been described in Ref. 26. The $J_{\rm eff} = 1/2$ band structure shown in Ref. 26 includes tilting about [110] leading to a gap opening at some of the band crossing points in Fig. 2(i).

IV. MAGNETISM: MEAN-FIELD THEORY

The quasi-2D members of the Ruddelsden-Popper series of strontium iridates display novel $J_{\rm eff} = 1/2$ magnetism. To understand and to account for the differences between the magnetic ordering at low temperatures between the different compounds within a consistent picture, we study the effect of electronic interactions by supplementing our $J_{\rm eff} = 1/2$ tight-binding model with a Hubbard term of the form

$$H_{\rm int} = \tilde{U}\sum_i n_{i+}n_{i-}, \quad (14)$$

where $n_{i\pm}$ is the number operator for pseudospin $J_z = \pm 1/2$ at site i. The interaction strength $\tilde{U}$ in the $J_{\rm eff} = 1/2$ basis can be obtained from a multiorbital Hubbard model as $\tilde{U} = \frac{U}{3} + 2\frac{U'}{3} - 2\frac{J}{3}$, where U, U', and J are, respectively, the intraorbital repulsion, the interorbital repulsion, and Hund's coupling for

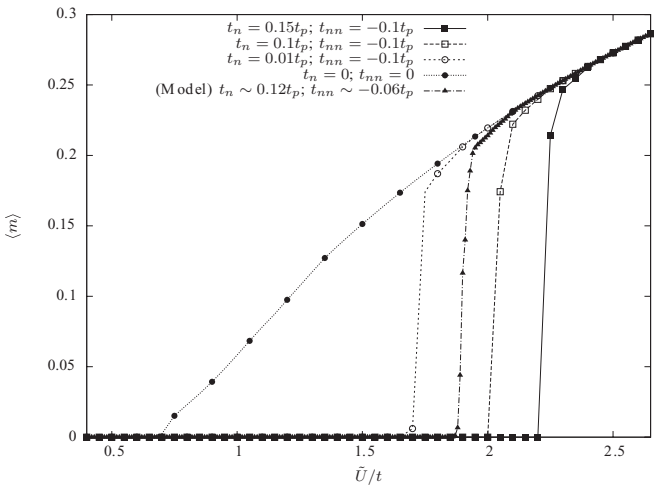

FIG. 4. Magnitude of order parameter as a function of $\tilde{U}/t$ for Sr-214. Various cases of t_n and t_{nn}, while keeping other parameters listed in Appendix B1, are presented. For $t_{nn} = t_n = 0$, the transition occurs at $0.7t$ and is second order. On the other hand, when they are finite, the critical interaction strength is larger and the transition is first-order.

t_{2g} orbitals. The Kanamori form[30] with $J = \frac{U-U'}{2}$ and[23] $U' = 0.8U$ was used in the rest of the paper.

Rewriting $H_{\rm int} = -\frac{2\tilde{U}}{3}(S_{ix}^2 + S_{iy}^2 + S_{iz}^2) + \frac{\tilde{U}}{2}\sum_i(n_{i+} + n_{i+})$, where S_{ix}, S_{iy}, and S_{iz} are the components of the pseudospin operator, it is clear that a mean-field decoupling in a magnetic channel such as $S_{i\alpha}^2 = 2m_{i\alpha}S_{i\alpha} - m_{i\alpha}^2$ with $\alpha = x,y,z$ can be employed. A self-consistent iteration to compute the mean-field parameters $m_{i\alpha}$ is carried out.

A. Magnetism in Sr-214

On increasing $\tilde{U}$, we find a first-order phase transition from a metallic state to a magnetically ordered insulating state as depicted in Fig. 4. The ordering pattern, shown in Fig. 1(a), has the order parameters $\vec{m}_B^1 = (-m_x, m_y, 0)$ for the blue sublattice in the first layer and $\vec{m}_R^1 = (m_y, -m_x, 0)$ for the red sublattice in the first layer. The ordering in the second layer is identical to the first, while the order parameters for the respective sublattices in the third and fourth layer are opposite in sign from those in the first and second layer.

Within the plane, the canting is such that the net ferromagnetic moment points in the [110] direction. Along the c axis, the net ferromagnetic moment shows an "up-up-down-down" pattern which is consistent with resonant x-ray scattering experiments[31] and remains unchanged upon taking the large-$\tilde{U}$ limit of our calculation.

For the set of parameters mentioned in Appendix B 1a, the critical interaction strength at which the magnetic transition occurs is $\tilde{U}_c \approx 1.91t$, where t is the magnitude of the Slater-Koster[32] hopping $t_{dd\pi}$. This critical interaction strength is quite sensitive to the strength of the next-nearest- and next-next-nearest-neighbor hopping, which control the dispersion along the high-symmetry direction M-X. In the limit where these hoppings are absent, the transition is second order. The critical interaction strength also decreases in this limit because of the large Fermi-surface nesting. By varying the strength of the

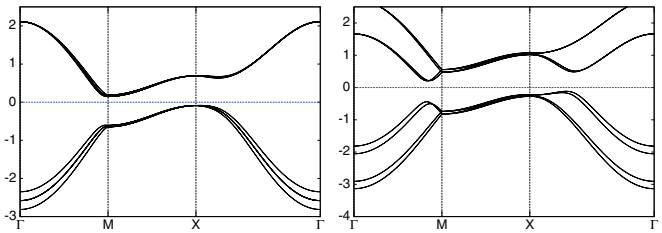

(a) Sr-214 (b) Sr-327

FIG. 5. (Color online) Band structure including Hubbard interaction in the $J_{\text{eff}} = 1/2$ basis for Sr-327 and Sr-214. In this figure, a $\tilde{U}$ value of $2.3t$ was used.

next-nearest-neighbor hopping strength between 0 and 0.17, the critical interaction strength can be tuned from $\tilde{U}_c \approx 0.7t$ and $\tilde{U}_c \approx 2.2t$ as shown in Fig. 4. Regardless of when the transition occurs, the size of the order parameters for a given $\tilde{U} > \tilde{U}_c$ (for fixed λ) is the same, implying that while the exact critical interaction $\tilde{U}_c$ hinges on the details of the band structure, the size of the order parameter only depends on $\tilde{U}$ within the $J_{\text{eff}} = 1/2$ model. It was shown that SOC and Hubbard U change the order parameter size in the t_{2g} model.[24]

The mean-field band structure for $\tilde{U} = 2.3t$ is shown in Fig. 5(a). The charge gap in this model is approximately $0.2t$. We see that ordering opens a gap for moderately large $\tilde{U}$, which in the weak-coupling mean-field treatment hints at Slater insulating behavior. A Slater transition is usually accompanied by translation symmetry breaking, but for this compound the staggered rotation of the oxygen octahedra has already broken this symmetry.

B. Magnetism in Sr-327

Sr-327, because of its structural similarity to Sr-214, was also expected to have a canted AF ground state. However, the net ferromagnetic moment in Sr-327 was found to be smaller than that of Sr-214,[15,33] although other studies suggest a different moment size.[34] We show here that the difference in the c-axis stacking, with octahedra in adjacent layers having opposite rotation, makes the c-axis collinear AF state lower in energy than the noncollinear state.

On increasing $\tilde{U}$, there is a second-order phase transition from a near spin-orbit insulator or metallic state to a magnetically ordered insulator as shown in Fig. 6. Unlike the single-layer case, the transition depends more on whether the underlying band structure is gapped or not than on the dispersion in the M-X direction. The ordering pattern, shown in Fig. 1(b), has the order parameters $\vec{m}^1_B = (0,0,m)$ for the blue sublattice in the first layer, and $\vec{m}^1_R = (0,0,-m)$ for the red sublattice in the first layer. The ordering in the second layer is identical to the first, and the order parameters for the respective sublattices in the second bilayer are identical and opposite in sign to those in the first bilayer. The ordering pattern can be understood from the terms in the spin model that we describe in Sec. V.

The unit cell contains two bilayers and there are two different almost degenerate collinear AF configurations possible for the ground state. We show one (slightly lower in energy) in Fig. 1(b); the other configuration has the same spin

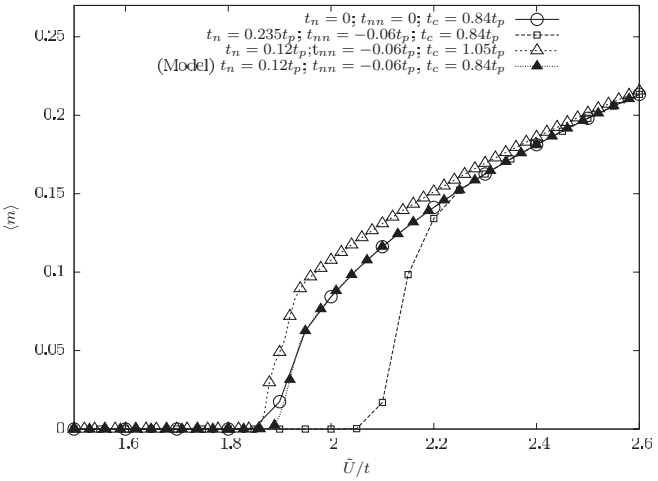

FIG. 6. Magnitude of order parameter as a function of $\tilde{U}/t$ for Sr-327. Results for different values of t_n, t_{nn}, and t_c, while keeping the other parameters listed in Appendix B1, are presented. The critical $\tilde{U}_c$ depends on mostly t_n and t_c, but the size of the moment is insensitive to the tight-binding parameters, once order has set in.

configuration for both bilayers. These two configurations were observed in the experiments of Ref. 35.

For the parameters used here, the critical interaction strength $\tilde{U}_c \approx 1.90t$. This critical interaction strength depends on the actual value of the next-nearest- and next-next-nearest-neighbor hoppings, similar to the single-layer case, but to a much lesser degree as shown in Fig. 6. Magnetic ordering does not change the dispersion but increases the direct gap.

C. Magnetism in Sr-113

Rotation and tilting of the octahedral environment around the Ir atom contributes more spin-dependent hopping terms in the $J_{\text{eff}} = 1/2$ basis in Sr-113 in comparison to its quasi-2D counterparts. These terms hint at a canted antiferromagnetic ground state with both in-plane and out-of-plane canting. The magnetic transition occurring at an interaction strength $\tilde{U}_c = 2.35t$ takes the system from a semimetal to a magnetic semimetal and then to a magnetic insulator with the magnetic pattern $\vec{m}_B = (m_x, m_y, m_z)$ for the blue sublattice, $\vec{m}_R = (-m_y, -m_x, m_z)$ for the red sublattice, $\vec{m}_Y = (-m_x, -m_y, m_z)$ for the yellow sublattice, and $\vec{m}_G = (m_y, m_x, m_z)$ for the green sublattice. The canting within each plane is equal and opposite for the different layers resulting in zero net in-plane moment, but there is a finite magnetic moment in the z direction.

The progression of the critical interaction strength $\tilde{U}_c$ required for a magnetic transition in the Ruddelsden-Popper series explains the experimentally observed MIT, as the number of layers is increased. In the current mean-field study, the magnetic ordering pattern does not change upon increasing $\tilde{U}$. To understand how our weak-coupling results above are related to the strong-coupling approach, spin models in the large-$\tilde{U}$ limit for Sr_2IrO_4 and $Sr_3Ir_2O_7$ are derived in the next section.

V. MAGNETISM: SPIN MODEL

For a general time-reversal invariant hopping between two sites given by $(t_{ll'} + i \sum_{\alpha = x,y,z} \sigma^\alpha t^\alpha_{ll'}) c^\dagger_{i,l,\sigma} c_{j,l'\sigma'}$, the

exchange Hamiltonian within second-order perturbation theory is

$$H = \sum_{\substack{\langle ij\rangle \\ ll'}} \left(J_{ij}^{ll'} \vec{S}_i^l \cdot \vec{S}_j^{l'} + \vec{D}_{ij}^{l,l'} \cdot \vec{S}_i^l \times \vec{S}_j^{l'} + \vec{S}_i^l \cdot \Gamma_{ij}^{l,l'} \cdot \vec{S}_j^{l'} \right), \quad (15)$$

with Heisenberg coupling $J_{ij}^{l,l'} = \frac{4}{\tilde{U}}(t_{l,l'}^2 - v_{l,l'}^2)$, Dzyaloshinskii-Moriya (DM) coupling $\vec{D}_{ij}^{l,l'} = \frac{4}{\tilde{U}}(2t_{l,l'}\vec{v}_{l,l'})$, and anisotropic exchange coupling $\Gamma_{ij,\alpha\beta}^{l,l'} = \frac{4}{\tilde{U}}(2v_{l,l'}^{\alpha} v_{l,l'}^{\beta})$. Here α,β are spin components and l,l' are layer indices.

For Sr-214, the nearest-neighbor exchange couplings within a layer are $J_p^{ll} = \frac{4}{\tilde{U}}(t_p^2 - t_p'^2)$, $\vec{D}_p^{ll} = \frac{8\epsilon_i t_p t_p'}{\tilde{U}}\hat{z}$, and $\Gamma_{p,zz}^{ll} = \frac{8}{\tilde{U}}t_p'^2$ for $l = 1,\ldots,4$, where ϵ_i in $\vec{D}_p^{ll}$ represents a change of sign between two adjacent bonds. Ignoring interlayer couplings, there is a canting angle at which the canted AF state is degenerate to the collinear AF state. This degeneracy arises because it is possible to turn the spin model into an isotropic Heisenberg model by an appropriate gauge transformation for the spin operators, as has been pointed out by others.[18,36]

We now add the interlayer couplings as a perturbation on the two degenerate states. Since each Ir atom has four neighbors in each adjacent layer, we separate the exchange terms into two types, between atoms of the same color (i.e., B to B) and between atoms of different colors (R to B). There are two hoppings of each kind, which we add together. For Sr-214, between layers 1 and 2, the exchange terms are $J_{BB}^{12} = \frac{4}{\tilde{U}}t_i^2$, $J_{BR}^{12} = \frac{4}{\tilde{U}}(t_{id}^2 - t_{iz}^2 - t_{iy}^2 - t_{ix}^2)$, $\vec{D}_{BR}^{12} = \frac{8}{\tilde{U}}(\pm t_{id}t_{ix}, \pm t_{id}t_{iy}, t_{id}t_{iz})$, and

$$\Gamma_{BR}^{12} = \frac{8}{\tilde{U}} \begin{pmatrix} t_{ix}^2 & t_{ix}t_{iy} & \pm t_{ix}t_{iz} \\ t_{ix}t_{iy} & t_{iy}^2 & \pm t_{iy}t_{iz} \\ \pm t_{ix}t_{iz} & \pm t_{iy}t_{iz} & t_{iz}^2 \end{pmatrix}.$$

Here, t_i is the interlayer hopping between B and B (or R and R), t_{id} between B and R, and pseudospin σ_a ($a = x,y,z$) dependent hopping between B and R is given by t_{ia}. The σ_x and σ_y dependent hopping between B (R) in layer 1 and the two R (B) in layer 2 have different signs, which we denote by $\pm$. This sign change means that these terms do not contribute to the energy if the magnetic unit cell is the same as the lattice unit cell. For layers 2 and 3, the exchange couplings are identical except a change in sign for the y component of the DM coupling ($D_{BR}^{23,y} = -D_{BR}^{12,y}$) and the xy and yz components of the anisotropic exchange ($\Gamma_{BR}^{23,xy} = -\Gamma_{BR}^{12,xy}$ and $\Gamma_{BR}^{23,yz} = -\Gamma_{BR}^{12,yz}$).

The lattice structure with four neighbors on the adjacent layer for each atom frustrates the DM and isotropic couplings. The canted AF state in an up-up-down-down fashion is favored by the anisotropic exchange, and this gets picked as the ground state, because the other terms are frustrated by the lattice.

In Sr-327, the bilayer couplings are much larger than the interbilayer couplings, hence only one bilayer is considered. The in-plane exchange couplings are identical to those of the single layer and the out-of-plane couplings are given by $J_c = \frac{4}{\tilde{U}}(t_z^2 - t_z'^2)$, $\vec{D}_c = \epsilon_i \frac{8}{\tilde{U}} t_z t_z' \hat{z}$, and $\Gamma_c^{zz} = \frac{8}{\tilde{U}}t_z'^2$, where t_z, and t_z' are, respectively, the pseudo-spin-independent and pseudo-spin-dependent bilayer hoppings described in Appendix B 1b. Unless $\frac{t_z'}{t_z} = \frac{t_p'}{t_p}$, the in-plane and out-of-plane DM couplings are frustrated, i.e., there is no spin configuration such that optimal canting is achieved for both of them. Thus, the relative strength of the bilayer hopping to the in-plane hopping decides the competition between canted AF and collinear AF. From the Slater-Koster method,[32] we estimate that $\frac{t_z'}{t_z} \approx 3\frac{t_p'}{t_p}$, picking out the c-axis collinear AF state as the ground state, which has been recently confirmed in experiments.[35,37–39]

The interlayer couplings favor an antiferromagnetic pattern between the same atoms of layers 2 and 3, as shown in Fig. 1, but this is close in energy to the ferromagnetic pattern, leading to the two possible arrangements discussed previously. It should be noted that the same conclusions for the magnetic ordering patterns were reached in other studies.[18,37,38] In the current study, the spin model was derived for the full unit cell, including four layers so that interlayer coupling is important, while those previous studies include Hund's coupling, which leads to the magnetic ordering pattern. Despite this difference, both approaches yield the same ordering pattern for both Sr-214 and Sr-327, and thus adding Hund's coupling would further stabilize the magnetic ordering pattern.

VI. DISCUSSION AND SUMMARY

We build a tight-binding model using t_{2g} orbitals for the different layered perovskite iridates in Sec. II to identify the states near the Fermi level to be made up of mostly $J_{\text{eff}} = 1/2$. We then construct a $J_{\text{eff}} = 1/2$ tight-binding model in Sec. III, and we study the magnetic order and MIT by taking into account Hubbard interactions within a mean-field approximation in Sec. IV. We find that our approach captures a rich phase diagram as $\tilde{U}$ increases: a first-order transition from a metal to a magnetic insulator for Sr-214, a transition from nearly a band insulator to a magnetic insulator for Sr-327, and a semimetal to magnetic insulator via a magnetic semimetal for Sr-113. The phase diagram for the different layered cases, sketched in Fig. 7, shows that the different members of the Ruddelsden-Popper series exhibit a different critical interaction U_c for a magnetic transition.

The magnetic ordering pattern in the ground state is intimately connected to the lattice structure. While the study in Ref. 24 does show the magnetic transition for Sr-214 and Sr-327 in an itinerant model, the current study with the full unit cell containing all the different layers in the $J_{\text{eff}} = 1/2$ model was performed to find the proper magnetic ordering pattern. In Sr-214, the interlayer isotropic Heisenberg and DM interactions are frustrated because Ir atoms in adjacent layers create a zero effective field due to their positions. Combined with the anisotropic exchange, this frustration selects the "up-up-down-down" pattern for the net ferromagnetic moment. Although these interlayer exchanges are small compared to the intralayer exchanges, they are significant because in their absence the coplanar CAF and collinear AF are degenerate within our $J_{\text{eff}} = 1/2$ model. In Sr-327, in contrast to Sr-214, the collinear AF state along the c axis is preferred because the bilayer nature of the lattice frustrates the DM interaction of each Ir atom with its five neighbours. However, this configuration is proximate in energy to the canted AF state,

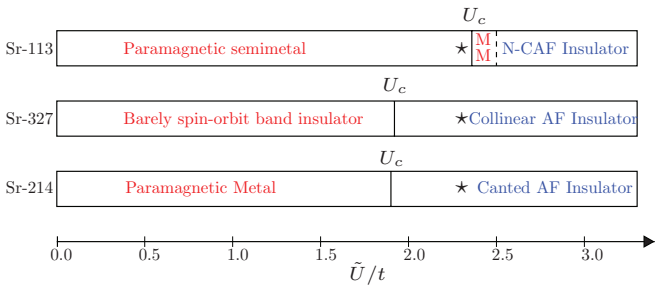

FIG. 7. (Color online) Phase diagram for the magnetic phases of the single-layer, bilayer, and three-dimensional compounds with the accompanying MIT. The critical value of $\tilde{U}$ at which the magnetic transition occurs for each compound is $\tilde{U}_c/t = 1.90$, 1.91, and 2.35, respectively. For Sr-214, due to the first-order nature of the transition, the system goes directly from metallic to insulating. For Sr-327, the magnetic ordering does not change the Fermi surface topology, but further increases the existing direct band gap. For Sr-113, the transition turns the metal into a magnetic metal (MM) before it develops a gap as the ordering increases. Sr-113 shows noncoplanar canted antiferromagnet (N-CAF) order, with the ferromagnetic moment pointing along the crystal c axis. In a scenario in which the Hubbard interaction is $2.3t \sim 0.46$ eV (setting $t \sim 200$ meV), the stars indicate where each compound should be on the phase diagram.

and spin dynamics as a function of temperature and magnetic field offer interesting subjects for future study.

For the iridates studied here, magnetic ordering patterns are identical to those given by the large $\tilde{U}$ limit spin model, implying that their Mott character cannot be corroborated by the ordering pattern. The proximity of the magnetic state to a metallic state points to Slater insulating behavior. The Slater mechanism is not obvious in Sr-214 because magnetic ordering does not spontaneously break translational symmetry, as the symmetry is already broken by the lattice structure. However, note that the unit cell doubling in Sr-214 does not open a full gap in the band structure, leaving degenerate bands along the line joining M-X in the Brillouin zone, which are then gapped out by the onset of magnetic order. Sr-327, on the other hand, is either a small-band-gap insulator or a metal with small Fermi surfaces at $\tilde{U} \approx 0.46$ eV, suggesting that the magnetic ordering is not due to Mott physics.

To summarize, we have studied the MIT in the layered iridates using mean-field theory. Our results suggest that magnetic ordering in the Ruddelsden-Popper series of strontium iridates is explained within weak-coupling theory. Magnetic ordering patterns obtained in the weak-coupling approach are continuously connected to the ordering patterns obtained in the large-$\tilde{U}$ spin model, suggesting that the iridates might be in the intermediate regime, which makes both approaches viable. In a similar context, it is interesting to note that iridium d orbitals look rather localized in resonant inelastic x-ray scattering,[31] but in a momentum space probe such as ARPES,[16,20,21], the d orbital bands are quite dispersive. While it is true that the effects of the Hubbard interactions are amplified due to the SOC, the magnetic ordering pattern itself is not sufficient to justify Mott physics in this series of iridates. Thus, one should look for a full charge gap above the magnetic ordering temperature to validate a strong Mott insulating picture. ARPES studies above and below the transition temperature might be one way to shed some light on the relation between charge gap and magnetic ordering and to pin down the strong correlation effect in these iridates.

ACKNOWLEDGMENTS

This work was supported by the NSERC of Canada. H.Y.K. acknowledges the Aspen Center for Physics where a part of the work was carried out.

APPENDIX A: DISPERSIONS AND TIGHT-BINDING PARAMETERS IN THE t_{2g} BASIS

The hopping parameters and dispersions for the t_{2g} tight-binding model for Sr-214, Sr-327, and Sr-113 mentioned in Sec. II are elaborated upon here.

1. Sr-214

The nearest-neighbor dispersions contained in H_{BB} are

$$\epsilon_n^{xy} = 2t[\cos(k_x) + \cos(k_y)], \tag{A1}$$

$$\epsilon_n^{yz} = 2[t_1 \cos(k_y) + t^\delta \cos(k_x)], \tag{A2}$$

$$\epsilon_n^{xz} = 2[t_1 \cos(k_x) + t^\delta \cos(k_y)], \tag{A3}$$

$$\epsilon^{\text{rot}} = 2t'[\cos(k_x) + \cos(k_y)], \tag{A4}$$

where the superscripts xy, xz, and yz denote the orbitals and t is the direct Slater-Koster overlap $t_{dd\pi}$ between the iridium d orbitals. t_1 and t^δ denote hopping integrals of d_{xz} (d_{yz}) to d_{xz} (d_{yz}) along the x (y) and y (x) axis, respectively. ϵ^{rot} arises from the nearest-neighbor overlap t' between d_{yz} and d_{xz} due to the rotation of oxygen octahedra. The next-nearest-neighbor dispersions making up $H_{BB/RR}$ are

$$\epsilon_d^{xy} = 4t_n \cos(k_x)\cos(k_y), \tag{A5}$$

$$\epsilon_d^{yz} = \epsilon^{xz} = 4t_{nd} \cos(k_x)\cos(k_y), \tag{A6}$$

$$\epsilon^{1d} = 4t_{1d} \sin(k_x)\sin(k_y), \tag{A7}$$

where t_n and t_{nd} represent intraorbital hopping between d_{xy} and $d_{xz/yz}$, respectively. ϵ^{1d} is hopping between d_{yz} (d_{xz}) and d_{xz} (d_{yz}) orbitals parametrized by an overlap t_{1d}. All the hopping parameters are obtained from Slater-Koster theory using the overlaps for the d orbitals $(t_{dd\pi}, t_{dd\sigma}, t_{dd\delta}) = (-1.0, 1.5, 0.25)$, a rotation angle of 12° for the IrO_6 octahedra, and a suppression factor of 0.2 for next-nearest-neighbor overlaps compared to nearest-neighbor overlaps. The parameter set obtained from the Slater-Koster method for the single layer model is then $(t, t_1, t', t_n, t_{1d}, t^\delta, t_{nd}) = (-1.0, -0.94, -0.15, 0.16, 0.11, 0.27, 0.0)$.

2. Sr-327

For Sr-327, within each layer, the dispersions and the tight-binding parameters are identical to those described for Sr-214 in Appendix A 1. The nearest neighbor overlaps between a blue (B)/red (R) atom and a red (R)/blue (B) atom in Eq. (5) were parametrized by $(t_z, t_z', t_z^\delta) = (-0.80, 0.36, -0.15)$. Here t_z is the intraorbital overlap between $d_{xz\,(yz)}$ orbitals, t_z^δ is between d_{xy} orbitals, and t_z' is the overlap between a $d_{yz\,(xz)}$ orbital on one atom and a $d_{xz\,(yz)}$ orbital on the Ir atom in the next layer.

The next-nearest-neighbor bilayer dispersions making up H_{BB}^{12} in Eq. (5) are $\epsilon_b^{yz} = 2\,t_{zn}\cos(k_y)$ and $\epsilon_b^{xz} = 2\,t_{zn}\cos(k_x)$, which are orbital diagonal with the parameter $t_{zn} = 0.2$.

3. Sr-113

Since the tilting of the octahedra along the [110] direction was ignored, Sr-113 differs from Sr-214 only in its c-axis dispersions. These intraorbital hoppings are $\epsilon_z = 2\,t_z\cos(k_z)$ for $d_{yz\,(xz)}$ orbitals and $\epsilon_z^{\delta} = 2\,t_z^{\delta}\cos(k_z)$ for the d_{xy} orbital with $t_z = -0.80$ and $t_z^{\delta} = 0.15$.

APPENDIX B: DERIVING $J_{\rm eff} = 1/2$ BASIS HOPPINGS FROM t_{2g} HOPPINGS

Consider a single bond with t_{2g} orbitals on each site with the overlaps between the various orbital combinations (these are diagonal in spin space) given by t_{yz}, t_{xz}, and t_{xy} for the intraorbital hoppings and t_{yz-xz}, t_{xz-yz}, t_{yz-xy}, t_{xy-yz}, t_{xz-xy}, and t_{xy-xz} for the interorbital hoppings. The $J_{\rm eff} = 1/2$ orbitals are given by $|J_z = \pm\frac{1}{2}\rangle = \frac{1}{\sqrt{3}}(|d_{yz}, \mp s\rangle \pm i|d_{xz}, \mp s\rangle \pm |d_{xy}, \pm s\rangle)$, and the time-reversal invariant hopping Hamiltonian for a bond is of the form $t\sigma^0 + i\sum_{\alpha=x,y,z} t^{\alpha}\sigma^{\alpha}$. From the t_{2g} overlaps, the parameters can be obtained as

$$t = \tfrac{1}{3}(t_{yz} + t_{xz} + t_{xy}), \tag{B1}$$

$$t^z = \tfrac{1}{3}(t_{yz-xz} - t_{xz-yz}), \tag{B2}$$

$$t^y = \tfrac{1}{3}(t_{xy-yz} - t_{yz-xy}), \tag{B3}$$

$$t^x = \tfrac{1}{3}(t_{xz-xy} - t_{xy-xz}). \tag{B4}$$

1. Dispersions in the $J_{\rm eff} = 1/2$ basis

a. Sr-214

For Sr-214, in Sec. III, we defined a Hamiltonian in Eq. (10) matrices A_k, B_k, and C_k. A_k describing hoppings within a layer was written as $\epsilon_k^a + \epsilon_k^{ad}\tau^x + \epsilon_k^{\prime ad}\tau^y\sigma^z$ with τ and σ representing the sublattice and pseudospin degrees of freedom, respectively. The dispersions in A_k are

$$\begin{aligned}
\epsilon_k^a &= 4t_n\cos(k_x)\cos(k_y) + 2t_{nn}[\cos(2k_x) + cos(2k_y)],\\
\epsilon_k^{ad} &= 2t_p[\cos(k_x) + \cos(k_y)],\\
\epsilon_k^{\prime ad} &= 2t_p'[\cos(k_x) + \cos(k_y)].
\end{aligned}$$

In the above, ϵ_k^a and ϵ_k^{ad} are pseudospin-preserving hopping between the same sublattice (next-nearest and next-next-nearest) and different sublattices, respectively. t_n and t_{nn} are next-nearest and next-next-nearest neighbor overlap orbitals and t_p is the nearest-neighbor overlap. $\epsilon_k^{\prime ad}$ is the pseudospin σ^z dependent hopping between different sublattices with overlap t_p'. The parameter set used was $(t_p,t_p',t_n,t_{nn}) = (-0.57,0.10,-0.067,0.033)$.

The interlayer hoppings between layers 1 and 2 (also 3 and 4) were denoted by $B_k = \epsilon_k^b + \epsilon_k^{bd}\tau_x + \epsilon_k^{bz}\tau_y\sigma_z + \epsilon_k^{by}\tau_y\sigma_y + \epsilon_k^{bx}\tau_y\sigma_x$, with the dispersions given by

$$\epsilon_k^b = 2t_i\cos[(k_x + k_y)/2], \tag{B5}$$

$$\epsilon_k^{bd} = 2t_{id}\cos[(k_x - k_y)/2], \tag{B6}$$

$$\epsilon_k^{bz} = 2t_i^z\cos[(k_x - k_y)/2], \tag{B7}$$

$$\epsilon_k^{by} = i2t_i^y\sin[(k_x - k_y)/2], \tag{B8}$$

$$\epsilon_k^{bx} = i2t_i^x\sin[(k_x - k_y)/2]. \tag{B9}$$

Here, t_i is the hopping between the same sublattice and the same J_z while t_{id} is the hopping between a different sublattice with the same J_z. The superscript x in t_i^x, for example, represents a pseudospin σ^x dependent hopping between two orbitals on different sublattices. The remaining interlayer hoppings between the second and third layers (also the fourth and first layers) were captured by $C_k = \epsilon_k^c + \epsilon_k^{cd}\tau_x + \epsilon_k^{cz}\tau_y\sigma_z + \epsilon_k^{cy}\tau_y\sigma_y + \epsilon_k^{cx}\tau_y\sigma_x$ with the dispersions given by

$$\epsilon_k^c = 2t_i\cos[(k_x - k_y)/2], \tag{B10}$$

$$\epsilon_k^{cd} = 2t_{id}\cos[(k_x + k_y)/2], \tag{B11}$$

$$\epsilon_k^{cz} = 2t_i^z\cos[(k_x + k_y)/2], \tag{B12}$$

$$\epsilon_k^{cy} = -i2t_i^y\sin[(k_x + k_y)/2], \tag{B13}$$

$$\epsilon_k^{cx} = i2t_i^x\sin[(k_x + k_y)/2]. \tag{B14}$$

These interlayer overlap parameters were obtained by a fit to the splitting of the bands seen in LDA calculations of Ref. 40. The parameters used were $(t_i,t_{id},t_{iz},t_{iy},t_{ix}) = (-0.029,-0.0275,-0.0135,-0.0095,0.0095)$.

b. Sr-327

For Sr-327, the matrices A_k and C_k are the same as those for Sr-214, but B_k differs because of the bilayer nature. B_k has the form $t_c\tau_x + t_c'\tau_y\sigma_x$ as described in Sec. III. These bilayer hoppings are given by $(t_c,t_c') = (-0.48,0.24)$ in units of t. These parameters can be obtained from overlaps in the t_{2g} basis described in Appendix A 2 as $t_c = \frac{1}{3}(2t_z + t_z^{\delta})$ and $t_c' = \frac{2}{3}t_z'$.

*hykee@physics.utoronto.ca

[1] M. Z. Hasan and C. L. Kane, Rev. Mod. Phys. **82**, 3045 (2010).
[2] X.-L. Qi and S.-C. Zhang, Rev. Mod. Phys. **83**, 1057 (2011).
[3] L. Balents, Nature (London) **464**, 199 (2010).
[4] M. J. Lawler, H.-Y. Kee, Y. B. Kim, and A. Vishwanath, Phys. Rev. Lett. **100**, 227201 (2008).
[5] G. Chen and L. Balents, Phys. Rev. B **78**, 094403 (2008).
[6] D. Pesin and L. Balents, Nat. Phys. **6**, 376 (2010).
[7] B.-J. Yang and Y. B. Kim, Phys. Rev. B **82**, 085111 (2010).
[8] X. Wan, A. M. Turner, A. Vishwanath, and S. Y. Savrasov, Phys. Rev. B **83**, 205101 (2011).
[9] H.-C. Jiang, Z.-C. Gu, X.-L. Qi, and S. Trebst, Phys. Rev. B **83**, 245104 (2011).
[10] D. Xiao, W. Zhu, Y. Ran, N. Nagaosa, and S. Okamoto, Nat. Commun. **2**, 596 (2011).

[11]W. Witczak-Krempa and Y. B. Kim, Phys. Rev. B **85**, 045124 (2012).
[12]M. K. Crawford, M. A. Subramanian, R. L. Harlow, J. A. Fernandez-Baca, Z. R. Wang, and D. C. Johnston, Phys. Rev. B **49**, 9198 (1994).
[13]G. Cao, J. Bolivar, S. McCall, J. E. Crow, and R. P. Guertin, Phys. Rev. B **57**, R11039 (1998).
[14]G. Cao, Y. Xin, C. S. Alexander, J. E. Crow, P. Schlottmann, M. K. Crawford, R. L. Harlow, and W. Marshall, Phys. Rev. B **66**, 214412 (2002).
[15]I. Nagai, Y. Yoshida, S. I. Ikeda, H. Matsuhata, H. Kito, and M. Kosaka, J. Phys.: Condens. Matter **19**, 136214 (2007).
[16]B. J. Kim, H. Jin, S. J. Moon, J.-Y. Kim, B.-G. Park, C. S. Leem, J. Yu, T. W. Noh, C. Kim, S.-J. Oh, J.-H. Park, V. Durairaj, G. Cao, and E. Rotenberg, Phys. Rev. Lett. **101**, 076402 (2008).
[17]S. J. Moon, H. Jin, K. W. Kim, W. S. Choi, Y. S. Lee, J. Yu, G. Cao, A. Sumi, H. Funakubo, C. Bernhard, and T. W. Noh, Phys. Rev. Lett. **101**, 226402 (2008).
[18]G. Jackeli and G. Khaliullin, Phys. Rev. Lett. **102**, 017205 (2009).
[19]B. J. Kim, H. Ohsumi, T. Komesu, S. Sakai, T. Morita, H. Takagi, and T. Arima, Science **323**, 1329 (2009).
[20]Q. Wang, Y. Cao, J. A. Waugh, S. R. Park, T. F. Qi, O. B. Korneta, G. Cao, and D. S. Dessau, arXiv:1210.4141 [cond-mat.str-el].
[21]B. M. Wojek, M. H. Berntsen, S. Boseggia, A. T. Boothroyd, D. Prabhakaran, D. F. McMorrow, H. M. Rønnow, J. Chang, and O. Tjernberg, J. Phys. Condens. Matter **24**, 5602 (2012).
[22]H. Watanabe, T. Shirakawa, and S. Yunoki, Phys. Rev. Lett. **105**, 216410 (2010).
[23]R. Arita, J. Kuneš, A. V. Kozhevnikov, A. G. Eguiluz, and M. Imada, Phys. Rev. Lett. **108**, 086403 (2012).
[24]J.-M. Carter and H.-Y. Kee, Phys. Rev. B **87**, 014433 (2013).
[25]P. Fazekas, *Lecture Notes on Electron Correlation and Magnetism*, Series in Modern Condensed Matter Physics, Vol. 5 (World Scientific, Singapore, 1999) .
[26]J.-M. Carter, V. V. Shankar, M. A. Zeb, and H.-Y. Kee, Phys. Rev. B **85**, 115105 (2012).
[27]M. A. Subramanian, M. K. Crawford, and R. L. Harlow, Mater. Res. Bull. **29**, 645 (1994).
[28]J. M. Longo, J. A. Kafalas, and R. J. Arnott, J. Solid State Chem. **3**, 174 (1971).
[29]J. G. Zhao, L. X. Yang, Y. Yu, F. Y. Li, R. C. Yu, Z. Fang, L. C. Chen, and C. Q. Jin, J. Appl. Phys. **103**, 103706 (2008).
[30]J. Kanamori, Prog. Theor. Phys. **30**, 275 (1963).
[31]J. Kim, D. Casa, M. H. Upton, T. Gog, Y.-J. Kim, J. F. Mitchell, M. van Veenendaal, M. Daghofer, J. van den Brink, G. Khaliullin, and B. J. Kim, Phys. Rev. Lett. **108**, 177003 (2012).
[32]J. C. Slater and G. F. Koster, Phys. Rev. **94**, 1498 (1954).
[33]S. Fujiyama, K. Ohashi, H. Ohsumi, K. Sugimoto, T. Takayama, T. Komesu, M. Takata, T. Arima, and H. Takagi, Phys. Rev. B **86**, 174414 (2012).
[34]C. Dhital, S. Khadka, Z. Yamani, C. de la Cruz, T. C. Hogan, S. M. Disseler, M. Pokharel, K. C. Lukas, W. Tian, C. P. Opeil, Z. Wang, and S. D. Wilson, Phys. Rev. B **86**, 100401 (2012).
[35]S. Boseggia, R. Springell, H. C. Walker, A. T. Boothroyd, D. Prabhakaran, D. Wermeille, L. Bouchenoire, S. P. Collins, and D. F. McMorrow, Phys. Rev. B **85**, 184432 (2012).
[36]F. Wang and T. Senthil, Phys. Rev. Lett. **106**, 136402 (2011).
[37]J. W. Kim, Y. Choi, J. Kim, J. F. Mitchell, G. Jackeli, M. Daghofer, J. van den Brink, G. Khaliullin, and B. J. Kim, Phys. Rev. Lett. **109**, 037204 (2012).
[38]J. Kim, A. H. Said, D. Casa, M. H. Upton, T. Gog, M. Daghofer, G. Jackeli, J. van den Brink, G. Khaliullin, and B. J. Kim, Phys. Rev. Lett. **109**, 157402 (2012).
[39]J. P. Clancy, K. W. Plumb, C. S. Nelson, Z. Islam, G. Cao, T. Qi, and Y.-J. Kim, arXiv:1207.0960 [cond-mat.str-el].
[40]C. Martins, M. Aichhorn, L. Vaugier, and S. Biermann, Phys. Rev. Lett. **107**, 266404 (2011).
[41]This has been treated in Ref. 26.